Available online at www.sciencedirect.com
ScienceDirect
Acta Materialia 57 (2009) 4248–4260
Acta MATERIALIA
www.elsevier.com/locate/actamat

Microstructural evolution of cast Mg–Al–Zn during friction stir processing and subsequent aging

A.H. Feng, Z.Y. Ma *

Shenyang National Laboratory for Materials Science, Institute of Metal Research, Chinese Academy of Sciences, 72 Wenhua Road, Shenyang 110016, China

Received 25 February 2009; received in revised form 19 May 2009; accepted 21 May 2009
Available online 21 June 2009

Abstract

Mg–Al–Zn casting was subjected to two friction stir processing (FSP) protocols: single-pass with a pre-solution treatment (Pre-ST) and two-pass. Both the two-pass FSP and Pre-ST FSP produced uniform recrystallized microstructures with similar grain sizes of 7.5–8.7 μm and high ratios of high-angle grain boundaries of 95.9–97.5%; however, the boundary misorientation distributions were quite different for the two samples. For the Pre-ST FSP sample, a significant proportion of $\{10\bar{1}2\}$ twins were operative, with a complex and significantly weakened texture component. The mechanism of dynamic recrystallization (DRX) was mainly twinning DRX and continuous DRX (CDRX). However, for the two-pass FSP sample, the twins were significantly reduced, with a simple $\langle 0\,0\,0\,2\rangle$ texture component, and DRX was mainly associated with CDRX and discontinuous DRX. A post-FSP aging resulted in the precipitation of β-$Mg_{17}Al_{12}$ phase in continuous and discontinuous forms. Most of the continuous precipitates had a Burgers orientation relationship, namely: $(0001)_{Mg}\|(1\,1\,0)_{Mg_{17}Al_{12}}$, $[1\bar{2}10]_{Mg}\|[1\bar{1}1]_{Mg_{17}Al_{12}}$. The origin of the different microstructural characteristics in the two samples was discussed.

Keywords: Friction stir processing; Magnesium alloys; Recrystallization; Twinning; Grain refining

1. Introduction

Slip, twinning and kinking are significant mechanisms of plastic flow [1]. Plastic deformation in magnesium and its alloys is strongly affected by the initial orientation of the crystals and the deformation conditions, i.e. temperature and strain rate [2–4]. Dislocation slip has been considered an important contribution to the formation of texture and twinning [5]. Magnesium has three operative dislocation Burgers vectors: $\langle a\rangle = \frac{1}{3}\langle 1\,1\,\bar{2}\,0\rangle$, $\langle c\rangle = [0\,0\,0\,1]$ and $\langle c+a\rangle = \frac{1}{3}\langle 1\,1\,\bar{2}\,3\rangle$. Research into deformation twinning has recently attracted much attention [6,7]. Stacking fault energy (SFE), the most significant material parameter, affects the propensity of a material to form deformation twins [8].

Magnesium alloys exhibit low ductility due to the limited number of independent slip systems in the hexagonal close-packed (hcp) crystal structure [9]. The low SFEs of the magnesium alloys (60–78 mJ m^{-2} [10]) increase the difficulty of cross-slip, and therefore favor deformation twinning. Deformation twinning is known to play an important role in plastic deformation of the magnesium alloys over a wide temperature range [7,11]. Slip and twinning are considered as competitive mechanisms for plastic deformation [12]. In the hcp structure, deformation twinning occurs in the grains resisting basal slip and reorients the lattice to facilitate such slip [11]. Deformation twinning contributes to texture evolution by reorienting the twinned areas of the grains [13]. Furthermore, deformation twinning, whether formed under quasi-static or due to high-strain-rate deformation loading conditions, can effectively strengthen a material under some circumstances and weaken it under others. This complexity results mainly from the intricate interrelationships between slip, twinning and fracture processes of the hcp metals [7].

Friction stir processing (FSP) is a relatively novel metal-working technique, developed based on the basic principle

* Corresponding author. Tel./fax: +86 24 83978908.
E-mail address: zyma@imr.ac.cn (Z.Y. Ma).

1359-6454/$36.00 © 2009 Acta Materialia Inc. Published by Elsevier Ltd. All rights reserved.
doi:10.1016/j.actamat.2009.05.022

of friction stir welding (FSW) [14,15]. FSP causes intense plastic deformation, material mixing and thermal exposure, resulting in significant microstructural refinement, densification and homogenization of the processed zone [16]. FSP has currently attracted extensive attention for producing the fine-grained materials [17] and surface composites [18], and modifying the microstructure of heterogeneous metallic materials [16,19].

In the past few years, several studies have been conducted to understand the effect of FSP on the microstructure and properties of Mg–Al–Zn (AZ) magnesium alloys [20–24]. It was reported that effective microstructural homogenization and refinement could be achieved via FSP as a result of severe plastic deformation and dynamic recrystallization (DRX). Several aspects of the FSP AZ magnesium alloys were studied with emphasis on the effect of FSP parameters on the mechanical properties [20], the temperature distribution in the stir zone (SZ) [21], ultra-fine-grained structure [22], texture [23] and superplasticity [24]. However, inspection shows that understanding of the effect of FSP on the breakup and dissolution of the coarse network-like β-$Mg_{17}Al_{12}$ phase and the recrystallization process in cast AZ magnesium alloys with higher aluminum content is lacking.

Our previous work has indicated that FSP resulted in not only significant grain refinement, but also breakage and dissolution of most of the coarse network-like β-$Mg_{17}Al_{12}$ phase, and two-pass FSP combined with a subsequent aging is a simple and effective approach to improving the mechanical properties of AZ91D casting [25]. More recently, a detailed comparative study indicated that single-pass FSP on AZ80 casting produced a heterogeneous microstructure with low strength and ductility; however, both two-pass FSP and single-pass FSP with a pre-solution treatment (referred to hereafter as Pre-ST FSP) resulted in significantly improved microstructural uniformity and mechanical properties [26]. These studies demonstrate that two-pass FSP is a highly effective approach to enhancing the mechanical properties of AZ magnesium alloy castings. Furthermore, it was revealed that the two-pass FSP AZ80 exhibited more uniform microstructure and better mechanical properties than the Pre-ST FSP AZ80 [26]. Considering the fact that the two-pass FSP AZ80 sample had quite different microstructures prior to the final FSP pass, compared to the Pre-ST FSP sample [26], it is very likely that two FSP AZ80 samples would exhibit different deformation and recrystallization mechanisms. Furthermore, only limited investigation of the precipitation behavior of FSP AZ magnesium alloys has been undertaken [26]. Therefore, it is worthwhile to conduct in-depth microstructural examinations on the AZ magnesium alloys after FSP and subsequent aging.

In this study, the FSP AZ80 castings, prepared by both single-pass FSP with a Pre-ST and two-pass FSP, were subjected to detailed microstructural examinations. The aim is (i) to examine the effect of the FSP procedures on the grain boundary (GB) characteristics; (ii) to elucidate the operative recrystallization mechanism in the AZ magnesium alloys during FSP; and (iii) to develop an understanding of the precipitation behavior in supersaturated AZ magnesium alloys induced by FSP.

2. Materials and methods

As-cast AZ80 alloy billet with a composition of 8.5Al–0.5Zn–0.12Mn (wt.%) was used in this study. 8 mm thick plates were machined from the billet and subjected to FSP at a tool rotation rate of 400 rpm and a traverse speed of 100 mm min^{-1}. A steel tool with a shoulder 24 mm in diameter and a threaded cylindrical pin 8 mm in diameter and 6 mm in length was used. Two FSP procedures were used in this experiment. The first is single-pass FSP with a Pre-ST at 415 °C for 16 h. The second is two-pass FSP with a 100% overlap and the same forward directions (hereafter referred to as the two-pass FSP sample).

The specimens for microstructural examinations were cross-sectioned perpendicular to the FSP direction. Microstructural characterization and analysis were carried out by scanning electron microscopy (SEM, Hitachi S-3400 N), electron backscattered diffraction (EBSD, HKL), transmission electron microscopy (TEM, FEI TECNAIG2), and high-resolution transmission electron microscopy (HREM). The specimens for SEM were prepared by mechanical polishing and etching using a solution of 3 g picric acid + 20 ml acetic acid + 50 ml ethanol + 20 ml water. The specimens for EBSD were prepared by electrochemical polishing with commercial AC2 electrolyte, produced by Struers Company, at 25 V and 20 °C. Texture analyses were carried out by recording the $\{0\,0\,0\,2\}$, $\{1\,0\,\bar{1}\,0\}$ and $\{1\,0\,\bar{1}\,1\}$ pole figures around the center of the SZ. The thin foils for TEM and HREM were prepared by the ion-milling technique.

The aging treatment was conducted at 177°C for various dwelling times (1–24 h). The age-hardening response was determined at intervals of 1 h by Vickers hardness measurements performed on a Leco-LM-247AT machine by applying a 200 g load for 10 s. Each reported hardness value is the average of five measurements along the mid-thickness of the cross-section in the SZ.

3. Results

The orientation map of the Pre-ST FSP sample is shown in Fig. 1a, where high-angle grain boundaries (HAGBs with grain misorientations $\geqslant 15°$) and low-angle grain boundaries (LAGBs with grain misorientations $<15°$) are depicted by black and white lines, respectively. The Pre-ST FSP sample was characterized by fine and uniform recrystallized grains (Fig. 1a). Further, the ratio of the HAGBs as high as 97.5 % was obtained (Fig. 1b). Misorientation axis distributions in the crystal coordinate system are also shown for some angular ranges at $30 \pm 5°$ and $86 \pm 5°$, respectively, in Fig. 1b. Furthermore, there are two prominent peaks in the misorientation angle distribu-

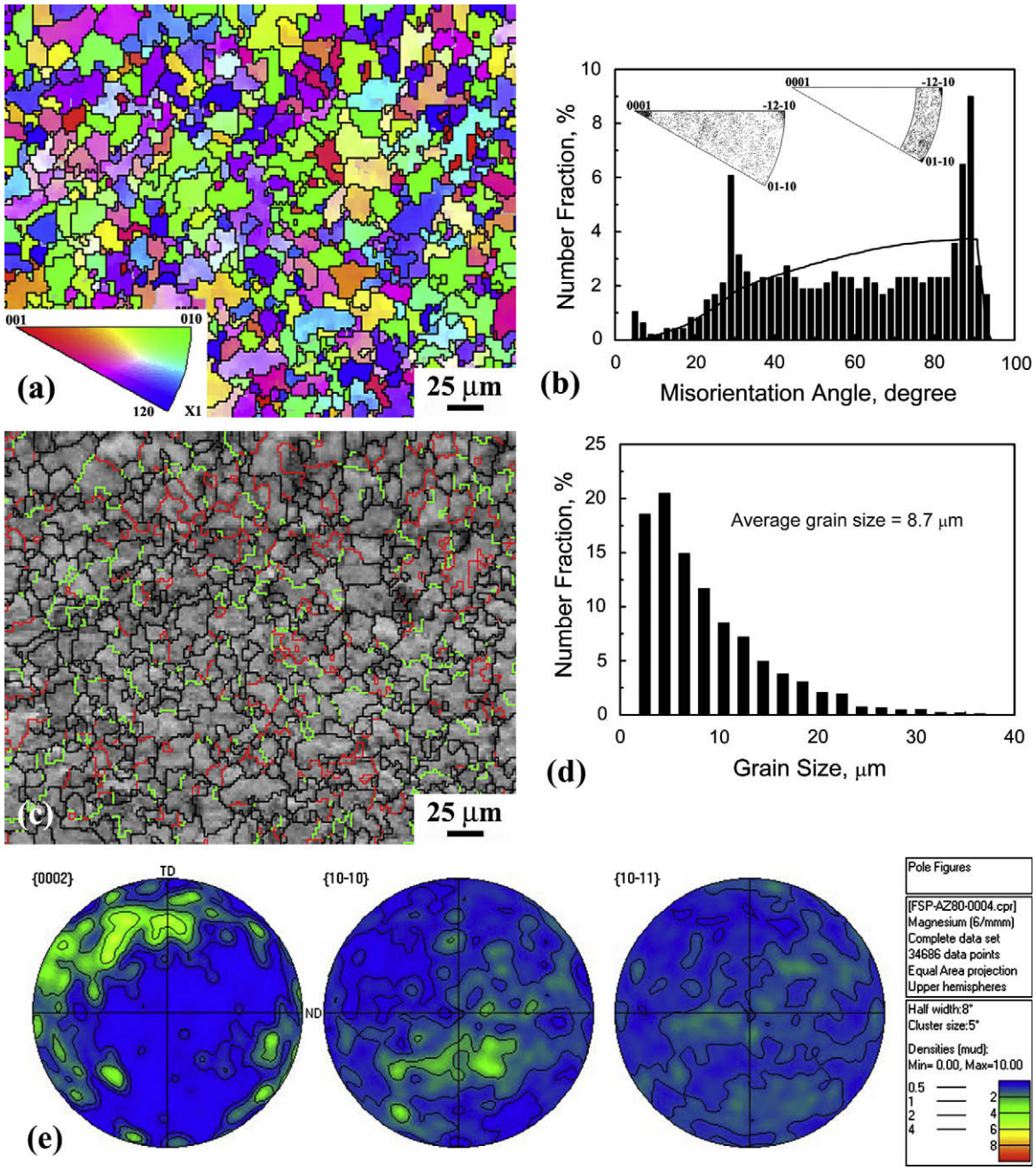

Fig. 1. EBSD maps of SZ in the Pre-ST FSP sample: (a) orientation map (see the unit triangle legend); (b) number fractions of misorientation angle; (c) Kikuchi contrast map, red boundaries represent $\{10\bar{1}2\}$ extension twins with a misorientation angle of $86 \pm 5°$ and green boundaries refer to boundaries with a misorientation angle of $30 \pm 5°$; (d) distribution of grain size; (e) $\{0002\}$, $\{10\bar{1}0\}$ and $\{10\bar{1}1\}$ pole figures (for interpretation of the references to colour in this figure legend, the reader is referred to the web version of this article).

tion, which is quite different from a random distribution of the hcp crystallites as shown in Fig. 1b by the black solid line [27]. The first peak is at $30 \pm 5°$ and the second peak is at $86 \pm 5°$. The fractions of the $30 \pm 5°$ and $86 \pm 5°$ boundaries were determined to be 21.3% and 28.0%, respectively. The Kikuchi contrast map shows the distribution of the boundaries with the misorientation angle of $86 \pm 5°$, corresponding to $\{10\bar{1}2\}$ twin boundaries (TBs, red lines) and $30 \pm 5°$ (green lines), respectively (Fig. 1c). A histogram of the grain size in the Pre-ST FSP sample is shown in Fig. 1d. The average grain size was determined to be 8.7 μm. Fig. 1e shows the $\{0002\}$, $\{10\bar{1}0\}$ and $\{10\bar{1}1\}$ pole figures of the Pre-ST FSP sample. A weakened and complex texture component was observed.

The orientation map of the two-pass FSP sample is shown in Fig. 2a. The ratio of the HAGBs was determined to be 95.9% (Fig. 2b). A prominent peak at $30 \pm 5°$ was observed in the misorientation angle distribution (Fig. 2b). The fractions of $30 \pm 5°$ and $86 \pm 5°$ boundaries were 34.5% and 7.6%, respectively. The distribution of the

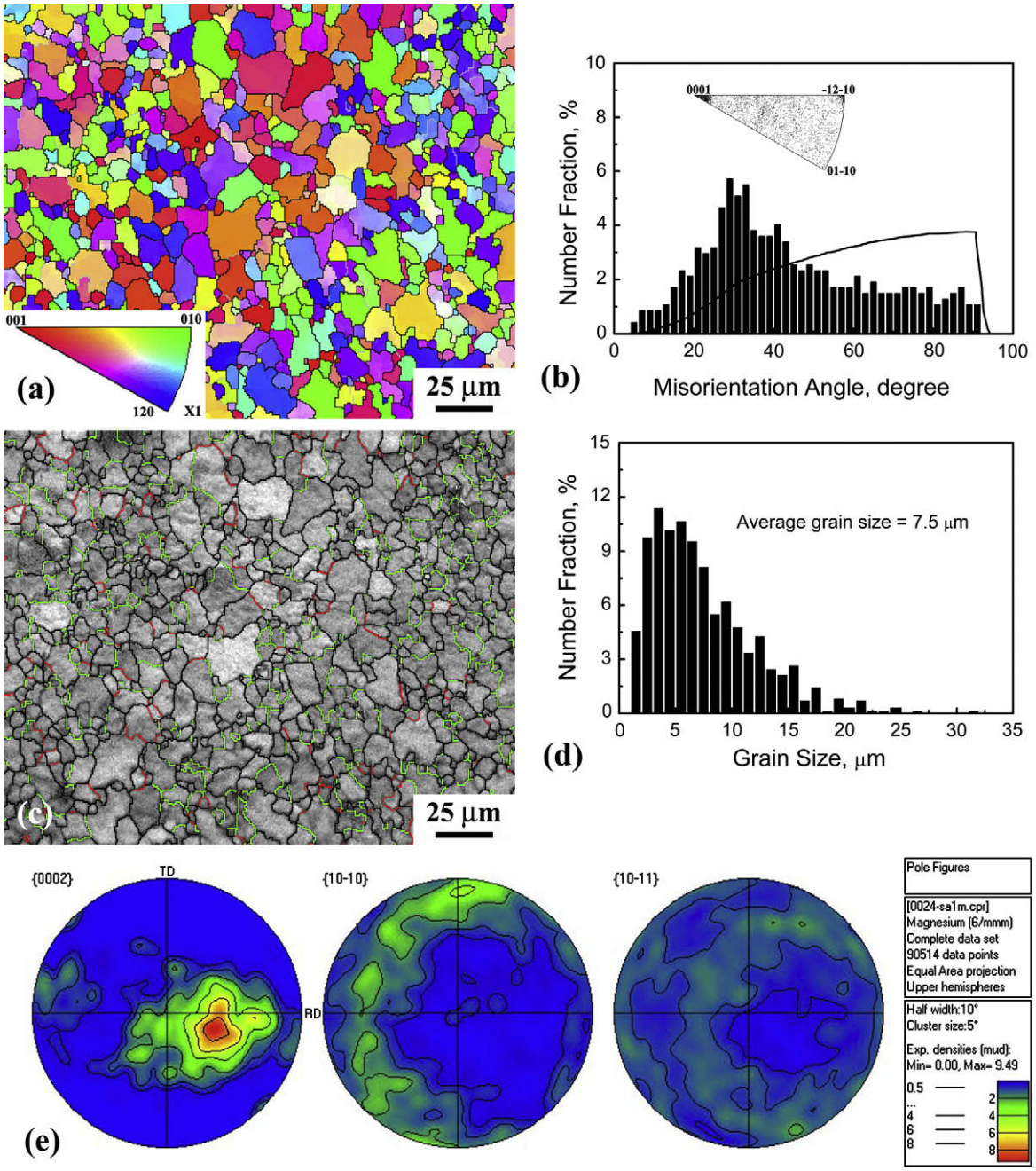

Fig. 2. EBSD maps of SZ in the two-pass FSP sample: (a) orientation map (see the unit triangle legend); (b) number fractions of misorientation angle; (c) Kikuchi contrast map, red boundaries represent $\{10\bar{1}2\}$ extension twins with a misorientation angle of $86 \pm 5°$ and green boundaries refer to boundaries with a misorientation angle of $30 \pm 5°$; (d) distribution of grain size; (e) $\{0002\}$, $\{10\bar{1}0\}$ and $\{10\bar{1}1\}$ pole figures. (for interpretation of the references to colour in this figure legend, the reader is referred to the web version of this article).

$\{10\bar{1}2\}$ TBs (red lines) and the boundaries with the misorientation angle of $30 \pm 5°$ (green lines) is shown in Fig. 2c. The average grain size was determined to be 7.5 μm (Fig. 1d). A simple $\langle 0\,0\,0\,2 \rangle$ texture component was observed (Fig. 2e).

In the Pre-ST FSP sample, multiple twins with some being intersected were frequently observed (Fig. 3a). Fig. 3b shows the dark-field image of the deformation twins. Substructure and dense dislocations walls were clearly visible in Fig. 3c. Furthermore, the recrystallized grains were observed in Fig. 3d. The dislocations piled up against the original GBs, and were organized into the LAGBs (Fig. 3e). Fig. 4a shows HREM lattice image of the Pre-ST FSP sample with the $\{10\bar{1}2\}$ TB and the $[4\bar{2}\bar{2}\bar{1}]$ axis parallel to the electron beam. The second twinning and high densities of microtwins several atomic layers thick were also observed (Fig. 4b and c). In the two-pass FSP sample, twins were seldom observed. TEM examinations revealed the serrated recrystallized grains and subgrain structure (Fig. 5).

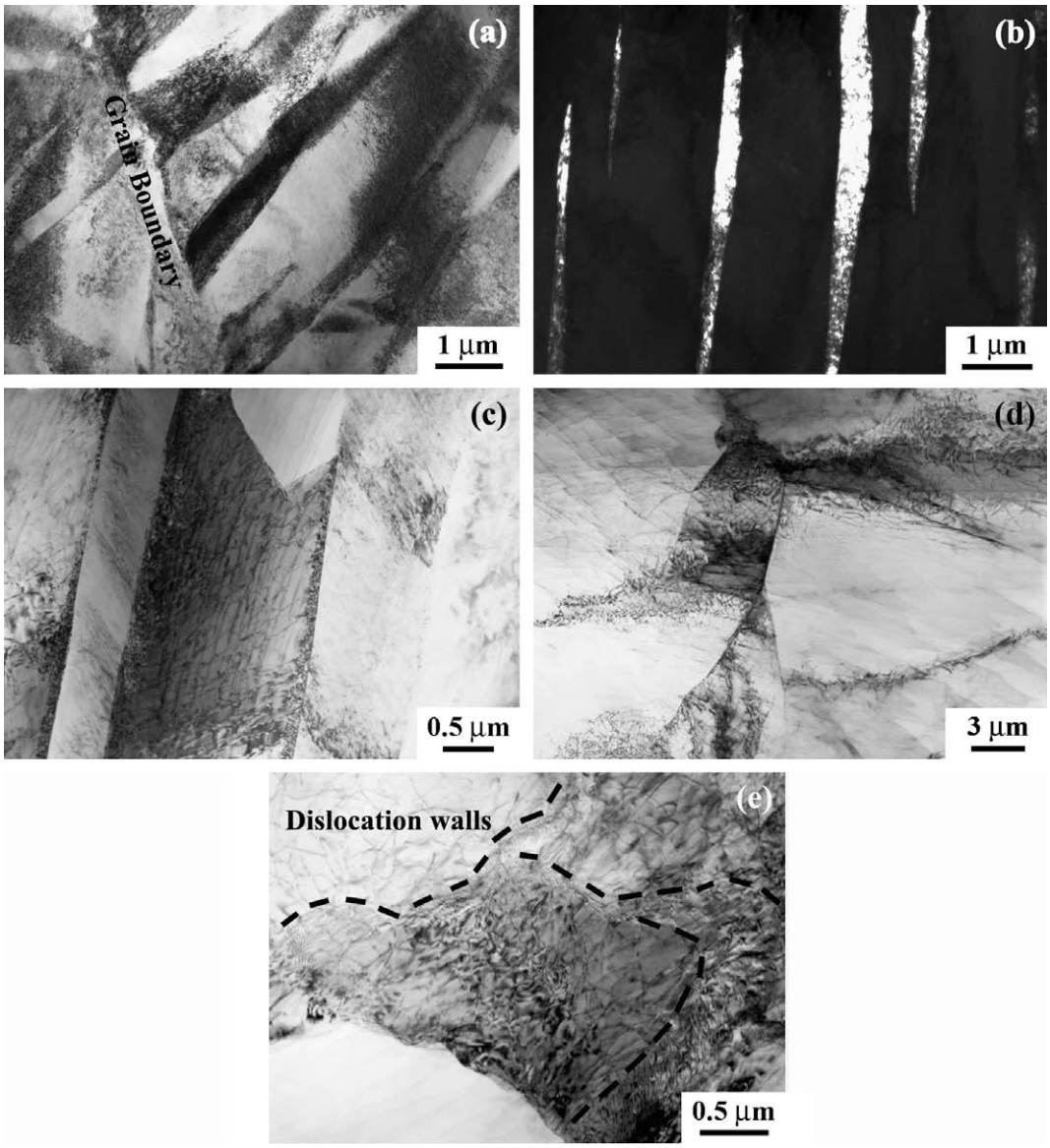

Fig. 3. TEM images in the SZ of Pre-ST FSP AZ80 magnesium alloy: (a) deformation twins; (b) dark-field image of deformation twins; (c) deformation twins and substructure; (d) recrystallized grains; (e) dislocation walls.

Fig. 6 shows the variation of Vickers hardness of the Pre-ST FSP sample with the aging time. The hardness increased as a function of the aging time before reaching the peak hardness. After aging for 10 h, the hardness reached a steady-state value of ~90 Hv. Increasing the aging time further did not change the hardness values of the sample. Therefore, an aging time of 10 h was chosen for the FSP samples in this study.

Fig. 7 shows SEM micrographs of the Pre-ST FSP sample aged at 177 °C for various times. In the initial aging stage of 3 h, discontinuous precipitation (DP) nodules were observed at the GBs and fine lozenge-shaped continuous precipitation (CP) plates appeared occasionally within some α-Mg grains (Fig. 7a). After aging for 10 h, the lamellar DP developed from the GBs into the grains, and the CP developed into laths inside the grains (Fig. 7b). Increasing the aging time further increased the fraction of DP nodules with an accompanying growth of the CP laths (Fig. 7c–f). In addition to the lamellar DP (shown by dark arrows), globular DP (shown by white arrows) was observed either at the original GBs or between the DP lamellae (Fig. 7d and f).

TEM examinations also revealed the existence of two types of precipitates in the aged Pre-ST FSP sample: CP and DP. Fig. 8a shows both lamellar and globular DPs, which were identified to be the body-centered cubic $Mg_{17}Al_{12}$ phase by corresponding selected-area diffraction pattern. Coarse DP lamellae grew initially from the GBs into the grains (point B). Furthermore, DP globules were observed around the lamellae (point A). Fine CP laths formed inside the α-Mg grains (Fig. 8b).

Similarly, in the aged two-pass FSP sample, it was observed that DP lamellae developed from the GBs into the grains, and fine CP laths formed within the grains

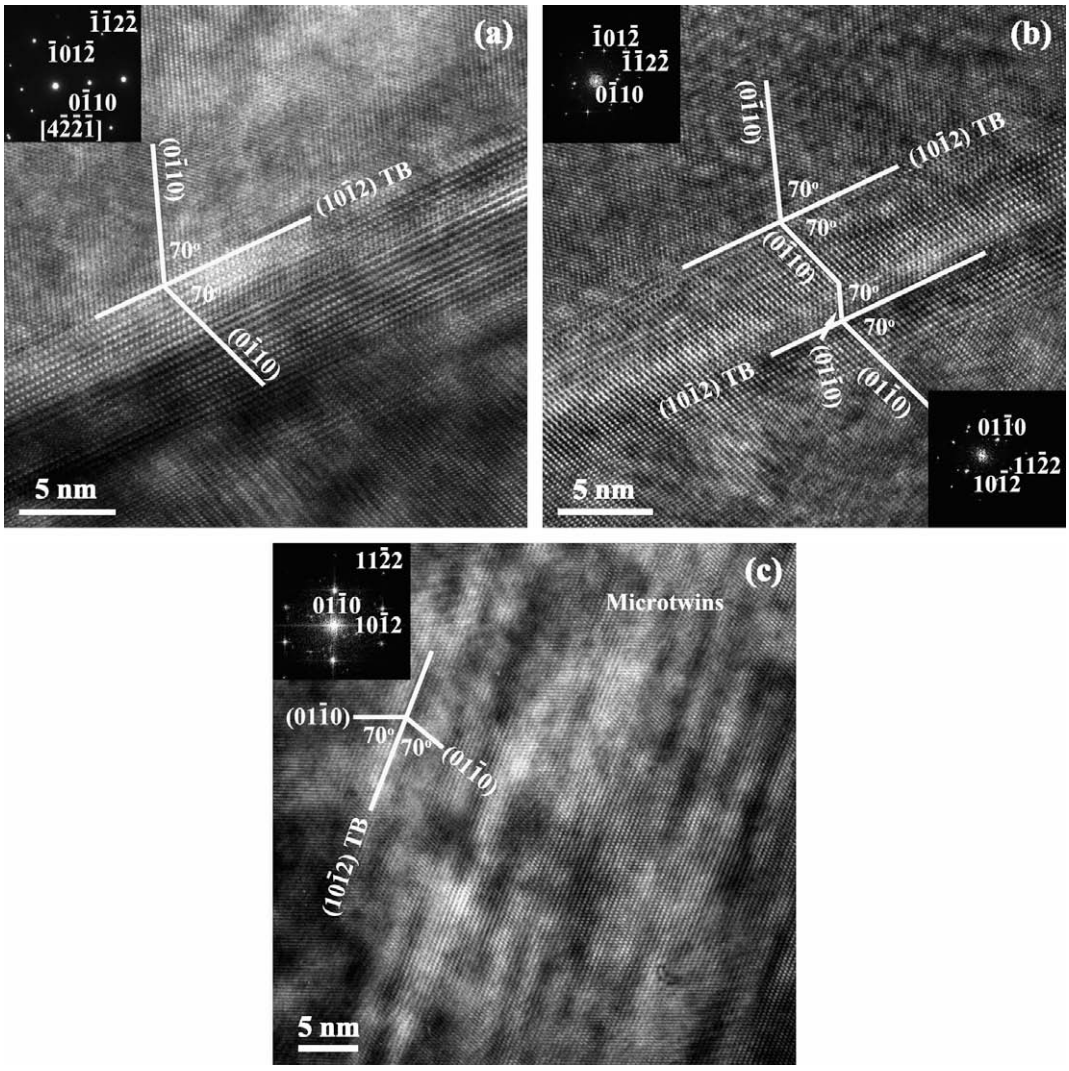

Fig. 4. HREM images of Fig. 3b in the SZ of Pre-ST FSP AZ80 magnesium alloy: (a and b) $\{10\bar{1}2\}$ TB; (c) microtwins.

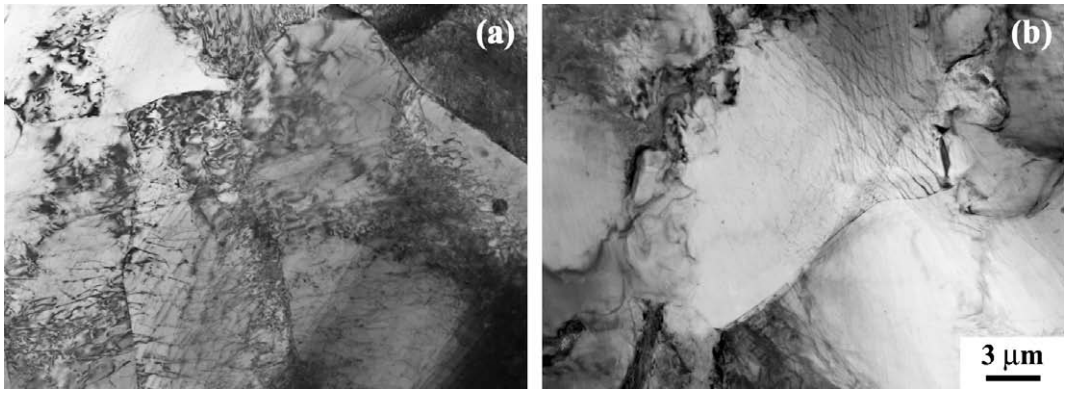

Fig. 5. TEM images of the two-pass FSP sample: (a) subgrain structure and (b) recrystallized grains.

(Fig. 9a). Furthermore, TEM examinations indicated that the boundary between the DP globules and CP laths was clearly visible in the aged two-pass FSP sample (Fig. 9b). The long CP laths formed a Widmanstätten morphology (Fig. 9c).

Fig. 10 shows the TEM and HREM images of the CP laths in the aged two-pass FSP sample. Parallel fine and long CP laths were distinctly visible (Fig. 10a). Most of the CP laths had a Burgers orientation relationship (OR): $(0001)_{Mg}\|(1\,1\,0)_{Mg_{17}Al_{12}}$ and $[\bar{1}\,2\,\bar{1}\,0]_{Mg}\|[1\,\bar{1}\,1]_{Mg_{17}Al_{12}}$

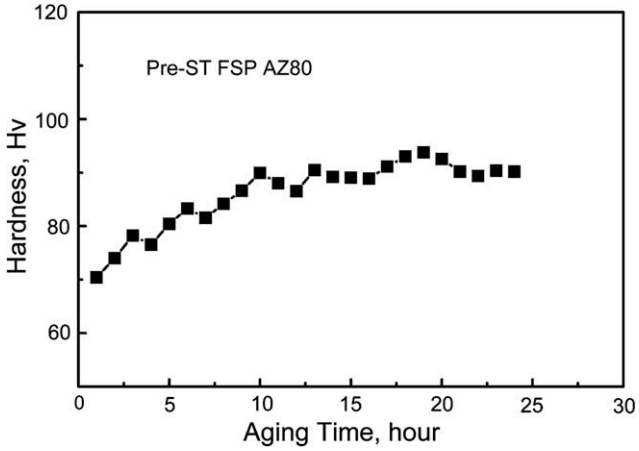

Fig. 6. Age-hardening curves of the Pre-ST FSP sample.

(Fig. 10b). The primary habit plane was parallel to the basal plane of the matrix.

4. Discussion

4.1. Microstructural characteristics

4.1.1. Grain boundary misorientation

A GB, characterized by five degrees of freedom [8], is defined as the surface between any two grains that have the same crystal structure and composition. Based on the symmetry operation, there are considered to be four types of GB [28]: twist, tilt, mixed and twin. The characteristics of the grain structure play an important role in determining various physical and mechanical properties [29]. It was well documented that FSP involves complex severe plastic

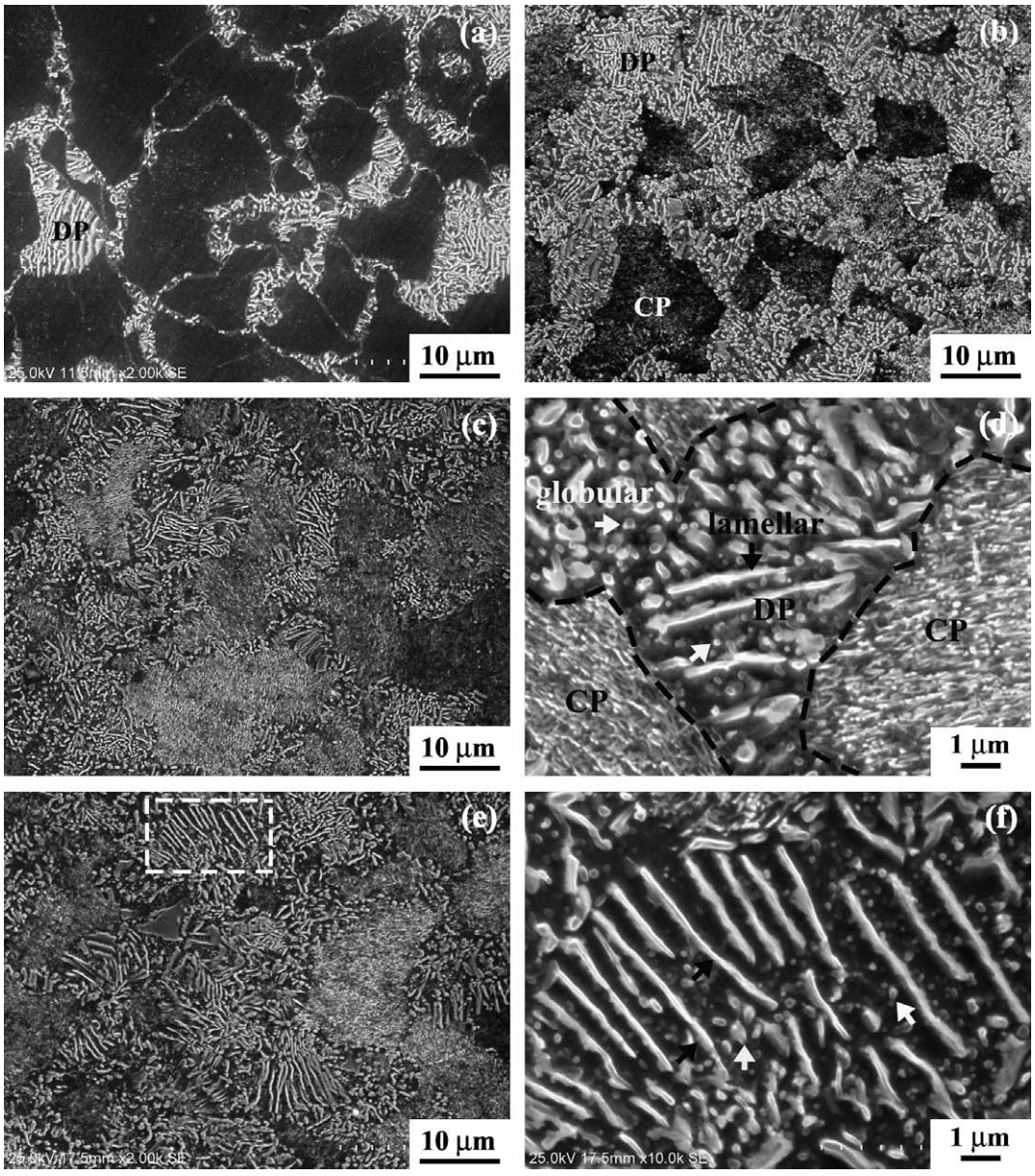

Fig. 7. SEM micrographs showing β-$Mg_{17}Al_{12}$ precipitates in Pre-ST FSP samples aged for (a) 3 h, (b) 10 h, (c) and (d) 19 h, (e) 24 h, and (f) a magnified view of rectangular zone in (e).

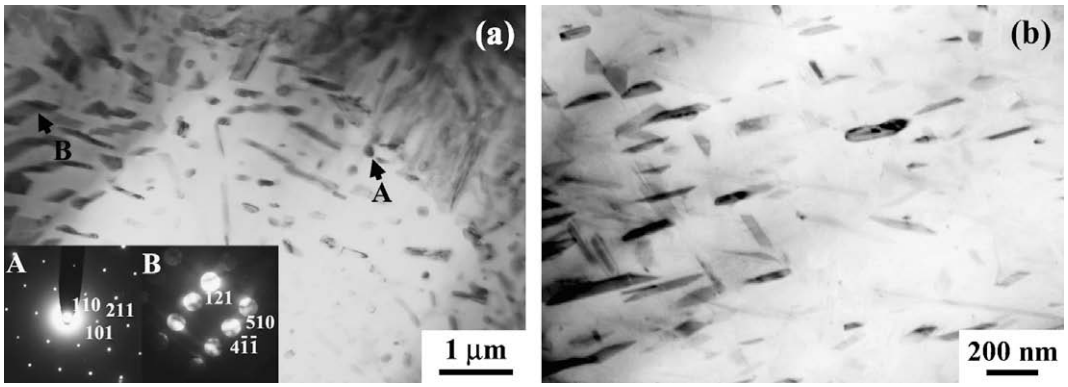

Fig. 8. TEM images showing two types of precipitates in aged Pre-ST FSP sample: (a) coarse DP lamellae and globular DP and (b) fine CP laths.

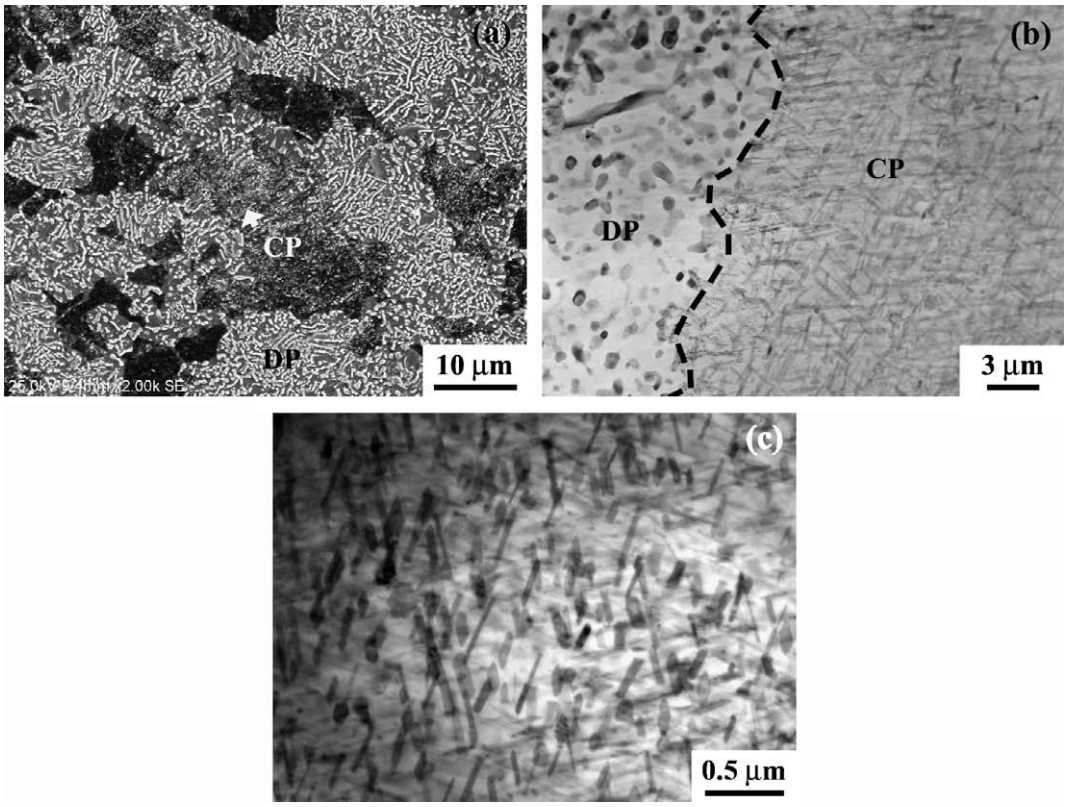

Fig. 9. Microstructure of aged two-pass FSP sample: (a) DP and CP; (b) boundary region of CP and DP; (c) TEM image showing Widmanstätten morphology of CP laths.

deformation and material movement. As a consequence, the material undergoes a substantial microstructural alteration, i.e. the crystallographic texture and various features of grain structure change greatly [30].

In this study, fine recrystallized grains were obtained in the Pre-ST and two-pass FSP samples and the average grain size was determined to be 8.7 and 7.5 μm, respectively, by EBSD. The grain sizes were obviously smaller than those estimated from optical micrographs [26]. This may be because the LAGBs could not be completely etched and therefore were not visible under optical microscopy. Furthermore, EBSD analyses indicated that the ratio of the HAGBs was as high as 97.5% and 95.9% for the Pre-ST and two-pass FSP samples, respectively (Figs. 1b and 2b). This indicated that DRX occurred during FSP due to intense plastic deformation and thermal exposure. Similarly, a high ratio of the HAGBs was reported in the SZ of FSW aluminum alloys [15]. A close examination of Figs. 1b and 2b indicates that there are prominent peaks in the misorientation angle distribution map for both the Pre-ST and two-pass FSP samples. These are different from the maps for the FSW aluminum alloys [31]. Recently, Stanford [32] reported that two peaks were observed in the misorientation histograms for compressed Mg–5Y–2Nd–2RE–

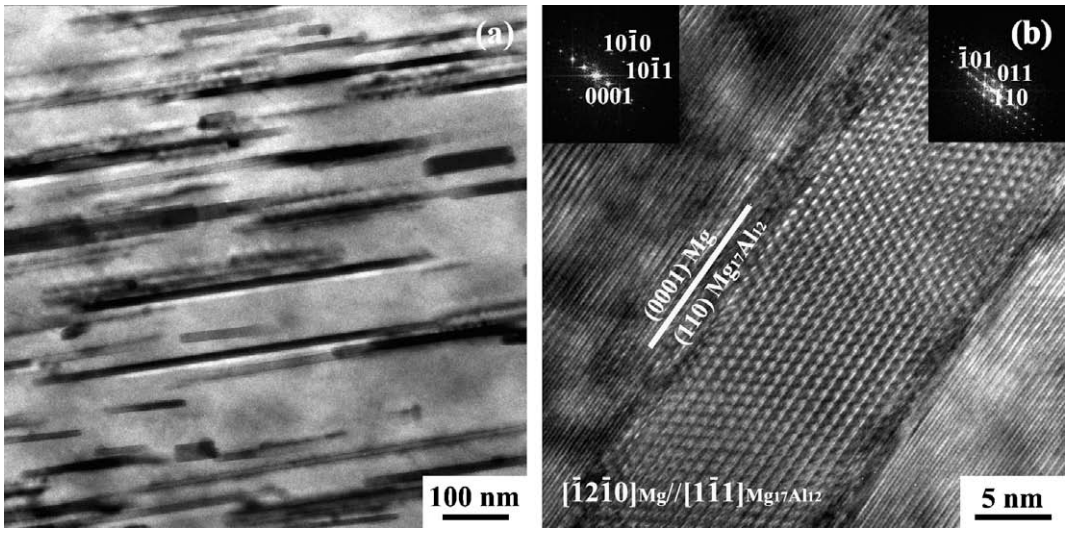

Fig. 10. TEM and HREM images of aged two-pass FSP sample showing: (a) fine and long CP laths and (b) $Mg/Mg_{17}Al_{12}$ interface viewed along the $[\bar{1}2\bar{1}0]_{Mg}\|[1\bar{1}1]_{Mg_{17}Al_{12}}$ zone axis.

0.5Zr (wt.%) alloy (known as WE54), i.e. one at ~85° to an axis of $\langle 1\bar{2}10\rangle$, corresponding to $\{10\bar{1}2\}$ twinning, and the other at ~35° misorientation to $\langle 10\bar{1}0\rangle$, referring to $\{11\bar{2}1\}$ twinning.

Magnesium and its alloys can deform by both slip and twinning. The characteristic misorientation relationships resulting from types of twinning commonly observed in magnesium are listed in Table 1 [33]. The first three result from single twinning on the $\{10\bar{1}1\}$, $\{10\bar{1}2\}$ and $\{10\bar{1}3\}$ planes. The remaining two result from double twinning.

For the Pre-ST FSP sample, there were two prominent peaks at $30\pm5°$ and $86\pm5°$ in the misorientation angle distribution map (Fig. 1b), with the fractions of the $30\pm5°$ and $86\pm5°$ boundaries being 21.3% and 28.0%, respectively. It is well known that following von Mises, a minimum of five independent systems must be active for an arbitrary shape change in any material [34]. The basic symmetry of the hcp crystals has the effect of limiting the number of independent slip systems, therefore making twinning an important deformation mechanism [35]. Twinning on the $\{10\bar{1}2\}$ pyramidal plane, one of the major twinning systems in magnesium alloys due to the smallest twinning shear ($s=0.1302$), leads to a small amount of expansion along the c-axis, with the basal plane in the twin being reoriented through 86° [35]. Fig. 11 shows the situation in magnesium before and after $\{10\bar{1}2\}$ twinning ($c/a=1.624$) [1]. Hence, the peak at 86±5° is attributable to a significant proportion of $\{10\bar{1}2\}$ twinning. On the other hand, the peak at $30\pm5°$ suggests that the most probable relative orientation of two adjacent grains belongs to the basal fiber texture [36].

Table 1
Misorientations about the $\langle 1\bar{2}10\rangle$ axis between the matrix and primary or secondary twins commonly observed in magnesium [33].

Type of twins	Misorientation angle (°)
$\{10\bar{1}1\}$	56
$\{10\bar{1}2\}$	86
$\{10\bar{1}3\}$	64
$\{10\bar{1}1\}-\{10\bar{1}2\}$	38
$\{10\bar{1}3\}-\{10\bar{1}2\}$	22

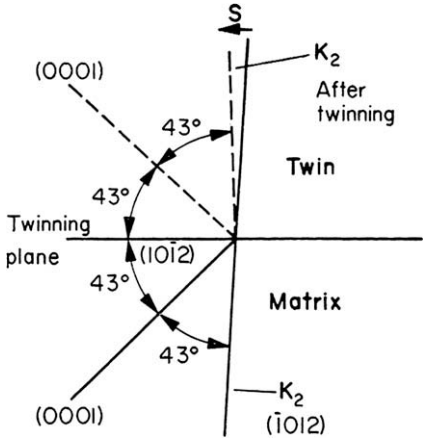

Fig. 11. Geometry of $\{10\bar{1}2\}$ twinning in hcp magnesium metal ($c/a=1.624$) [1].

Compared with the Pre-ST FSP sample, two main changes were observed in the two-pass FSP sample. First, the fraction of the $86\pm5°$ boundaries decreased to 7.6%, indicating that the $\{10\bar{1}2\}$ deformation twinning was significantly reduced. Second, the fraction of the boundaries with a misorientation angle of $30\pm5°$ increased to 34.5%. This indicates that the basal fiber texture in the two-pass FSP sample is much stronger than that in the Pre-ST FSP sample. This is consistent with Figs. 1e and 2e.

4.1.2. Recrystallization mechanism

The usual definition of recrystallization is the formation and migration of the HAGBs driven by the stored energy

of deformation [37]. The recrystallization is a nucleation and growth process. Favored sites for the recrystallization nuclei include the GBs, phase interfaces, twins, deformation bands and the surface of the materials, which are characterized as regions of heavy distortion, high dislocation density or strong orientation gradients [1]. Nucleation with low to medium SFEs can occur frequently by twinning [11,38], subgrain rotation [39] and bulging [3,40]. The growth is accomplished by the migration of HAGBs [41]. The process for creating a new recrystallized grain by the bulging out of an existing GB within the deformed structure was recognized by Beck and Sperry and described as strain-induced boundary migration [42].

It is well documented that DRX generally predominates during hot deformation of the magnesium alloys due to the lower SFEs. Proposed recrystallization mechanisms include: low-temperature DRX (LTDRX) [3,4,43], twinning DRX (TDRX) [11,38], continuous DRX (CDRX) [39,44] and discontinuous DRX (DDRX) [3,40]. Recent studies have provided significant insight into the mechanisms of DRX in magnesium alloys. The mechanisms of DRX change with temperature and strain [3,4]. DRX is a typical characteristic in the SZ of the FSP magnesium alloys. However, limited information is available so far about the DRX mechanisms in FSP magnesium alloys.

4.1.2.1. Pre-ST FSP sample. The Pre-ST FSP AZ80 was characterized by fine and recrystallized grains (Fig. 1a), with a great number of deformation twins being observed (Fig. 3a–c). Twinning is an important deformation mode for the hcp crystals, especially at low temperature or for a coarse-grained (CG) structure. Sitdikov et al. [11] found that in CG magnesium, the mechanism of DRX was associated with twinning. The Pre-ST prior to FSP resulted in significant grain coarsening, producing CG magnesium with an average grain size of ~420 μm [26]. Twinning-induced DRX occurred during subsequent FSP. EBSD results indicated that a significant proportion of $\{10\bar{1}2\}$ deformation twinning occurred in the Pre-ST FSP sample (Fig. 1). The dislocations and substructures were observed in the top of twin plates, indicating that, besides twinning, dislocation slip also contributed to the plastic deformation (Fig. 3c).

Such a "twin" DRX was associated with the following processes [11]: (i) the nucleation occurred either through the intersection of various systems of twins or the rearrangement of lattice dislocations within the twin lamellae; and (ii) the TBs were changed into random HAGBs at high strain due to their interaction with mobile dislocations. A unique characteristic of twinning is the larger grain size dependence of the twinning stress, compared to the slip stress [45]. A recent study by Danaf et al. [46] reconfirmed the significant effect of the grain size on the propensity for twinning. A 70/30 brass with a grain size of 250 μm showed a much greater twinning density than that with the grain sizes of 9 and 30 μm [12]. Gray [47] reported a greater propensity for mechanical twinning of larger grain sized high-purity Ti alloy (240 μm) than that of smaller grain sized high-purity Ti alloy (20 μm). Meyers et al. [12] showed that the twinning stress increased with decreasing grain size more than the stress required to activate the slip. Barnett et al. [48] found that there was a critical grain size for the twinning–slip transition.

It is well documented that the twinning deformation mode plays an important role during the deformation of hcp magnesium. Materials with hcp lattices exhibit many types of twinning (Table 1). HREM examinations indicated the existence of $\{10\bar{1}2\}$ TBs (Fig. 4). The $\{10\bar{1}2\}\langle 10\bar{1}1\rangle$ twin is activated by c-axis tension. The full description of the $\{10\bar{1}2\}$ deformation twinning mode is [6]:

$$K_1 = \{10\bar{1}2\}, \quad K_2 = \{\bar{1}012\}, \quad \eta_1 = \langle\bar{1}011\rangle,$$
$$\eta_2 = \langle\bar{1}01\bar{1}\rangle, \quad \gamma_0 = \frac{\sqrt{3}}{(c/a)} - \frac{(c/a)}{\sqrt{3}}, \tag{1}$$

where K_1, K_2, η_1 and η_2 have their usual meaning in twinning designation. The amount of shear γ_0 associated with twinning depends on the c/a ratio. For the materials with $c/a < \sqrt{3}$, the direction of shear is $[\bar{1}011]$, and the twinning occurs under tension parallel to the c-axis or under compression perpendicular to the c-axis. In magnesium and its alloys, there is a 43.15° angle between the basal $\{0002\}$ plane and the twinning $\{10\bar{1}2\}$ planes (Fig. 11).

Generally, twinning takes place at the early stages of plastic flow. Despite the limited contribution of twinning itself to the total plasticity, the abrupt change in orientation due to twinning may give rise to the reactivation of other slip systems [49]. When macro-twins are formed in a measurable volume fraction, second slip and twinning within the primary twins can make a sizeable contribution to the strain, provided that the slip–twin and twin–twin intersections are energetically feasible [50].

In the vicinity of initial GBs or TBs, the dislocations piled up to form LAGBs (Fig. 3c and e). Continuous absorption of dislocations on LAGBs results in the formation of HAGBs. This mechanism of the grain formation is CDRX. CDRX plays an important role at intermediate and high temperatures [3,4]. CDRX was found to involve dynamic polygonization in the rotated lattice regions adjacent to the initial boundaries [39]. Galiyev et al. [44] studied CDRX by measuring a gradual increase in the misorientations of subgrain boundaries using a conventional Kikuchi-line technique. CDRX can be attributed to dislocation slip in the mantle regions of initial grains [4]. During hot deformation, extensive cross-slip of the dislocations in the vicinity of pre-existing HAGBs gives rise to the formation of subgrains, and the cross-slip of the screw dislocations contributes to a rapid increase in misorientation [44].

4.1.2.2. Two-pass FSP sample. A previous study has indicated that the DRX mechanisms operative in magnesium are dependent on temperature and strain [3,4]. A map of DRX mechanisms revealed that in the temperature range

300–400 °C, the contribution of TDRX to the total recrystallization process tends to decrease and the contribution of CDRX increases with increasing temperature [4]. EBSD analyses indicated that the fraction of $86 \pm 5°$ boundaries in the two-pass FSP sample decreased to 7.6%, suggesting that the twinning was not a dominant DRX mechanism in the process of second-pass FSP. Fig. 5a indicates that continuous absorption of dislocations resulted in the formation of the high-angle subgrain boundaries (known as CDRX).

The recrystallized grains in the two-pass FSP sample exhibited serrated GBs (Fig. 5b). Tan et al. [51] found that the serrated or corrugated GBs would form at the early stage of DRX for rolled Mg–3Al–1Zn (wt.%). The serrated boundaries occur when the density of dislocations entering the GBs exceeds their absorption capacity or when the process of lattice dislocation absorption requires an incubation time [52]. Furthermore, the GB diffusion rate is faster for magnesium than for aluminum [53]. For the two-pass FSP AZ80, GBs become wavy and corrugated, indicating local migration of HAGBs, which is known as DDRX (Fig. 5b). Local migration of HAGBs occurred during plastic deformation in the temperature range of 300–450 °C, where the boundary mobility M becomes high [40].

Based on the above discussion, the mechanism of DRX in the two-pass FSP procedure might be mainly associated with CDRX and DDRX. Obviously, both TEM observations and EBSD analyses indicated that the mechanism of DRX in the two-pass FSP sample differed from that in the Pre-ST FSP sample. This difference in the recrystallization mechanism between the two FSP samples is mainly attributed to following reasons. First, the fine-grained structure in the single-pass FSP sample, compared to the CG structure in the Pre-ST sample, significantly reduced the contribution of twining during second-pass FSP, based on the study by Sitdikov et al. [11]. Second, the heat input of second-pass FSP for the two-pass FSP sample was higher than that of single-pass FSP for the Pre-ST FSP sample, because the deformation resistance of the single-pass FSP sample is larger than that of the Pre-ST sample. Based on the deformation mechanisms in magnesium, a temperature increase hinders deformation twinning and facilitates the operation of cross-slip and dislocation slip on multiple systems [4]. Sitdikov et al. [4] reported that extensive deformation twining took place at lower temperatures ranging from 20 to 350 °C. Galiyev et al. [3] found that the mechanisms of DRX depended on which deformation mechanism was operating, which varied with temperature.

4.1.3. Re-precipitation of fine β-$Mg_{17}Al_{12}$ phase

Our previous study indicated that FSP resulted in the breakage and dissolution of most of the coarse β-$Mg_{17}Al_{12}$ phase in the AZ80 casting, thereby producing an aluminum-supersaturated solid solution [26]. In many supersaturated binary alloys, such as Mg–Al alloys, precipitation take places either continuously or discontinuously [54]. For the Mg–Al alloys, the body-centered cubic $Mg_{17}Al_{12}$ phase precipitated as the equilibrium phase, without the formation of either GP zones or a transition lattice [55].

As shown in Figs. 7–9, the β-$Mg_{17}Al_{12}$ phase precipitated in the form of the DP and CP in both the aged Pre-ST and two-pass FSP samples. The DP, also known as cellular precipitation because the composition of the matrix changes discontinuously as the cell front passes, nucleated at the HAGBs and grew via a diffusion mechanism [56,57]. The nucleation mechanisms of the DP were affected by the interfacial energy, chemical forces and capillarity forces [58]. The nucleation rate of the DP has been measured as a function of temperature, initial grain size and solute content [58]. Duly et al. [59,60] reported the regular and irregular growth of the DP in the Mg–Al alloys, preceded by the asymmetry in the aluminum solute concentration profile.

As shown in Fig. 7a, DP nodules formed in the initial stage of aging for the Pre-ST FSP sample. Baumann et al. [61] correlated the morphology of the DP nodules, i.e. the single seam and double seam, with their nucleation mechanism. The double-seam nodules were observed distinctly, which developed alternately on both sides of the GB (Fig. 7a). For both the Pre-ST FSP and two-pass FSP samples (Figs. 7 and 9), the DP generally diverged and exhibited a bush-like morphology.

Crawley et al. [62] reported two types of DPs: lamellar and globular DPs. The DP lamellae had the same growth habit and OR like most of the CPs. However, the DP globules displayed no defined OR or growth habit with the matrix. As shown in Figs. 7–9, the DP globules developed either at the original GBs or around the DP lamellae, causing a breakdown of the DP lamellae as well as the adjacent CP laths [62]. Crawley et al. [62] reported that the DP globules adjacent to the CPs were not coherent with the matrix.

The CPs nucleated and grew in the remaining regions of the matrix grains. The fine lozenge-shaped CP plates developed into laths inside the grains with increasing aging time (Fig. 7). Celotto [63] reported that while the length and width of the CP plates increased with the aging, the thickness did not change.

The ORs between the $Mg_{17}Al_{12}$ phase plates and magnesium matrix have been well characterized [63,64]. The predominant OR was reported to be the Burgers OR, namely: $(0\,0\,0\,1)_{Mg}\|(1\,1\,0)_{Mg_{17}Al_{12}}$ and $[1\,\bar{2}\,1\,0]_{Mg}\|[1\,\bar{1}\,1]_{Mg_{17}Al_{12}}$ [63]. Furthermore, two different ORs, i.e. $(0\,0\,0\,1)_{Mg}\|(1\,\bar{1}\,1)_{Mg_{17}Al_{12}}$ and $[1\,\bar{2}\,1\,0]_{Mg}\|[1\,\bar{1}\,\bar{2}]_{Mg_{17}Al_{12}}$, $(0\,\bar{2}\,1\,1)_{Mg}\|(1\,\bar{1}\,0)_{Mg_{17}Al_{12}}$ and $[1\,0\,\bar{1}\,0]_{Mg}\|[1\,1\,0]_{Mg_{17}Al_{12}}$ were also reported by other investigators [57,62,65]. The near Burgers OR has been confirmed by Duly and other investigators [65,66].

Fig. 12 shows schematically the geometry of six variants of the Burgers OR for the CP [64]. The basal plane of the matrix $(0\,0\,0\,1)_{Mg}$ and habit plane of the precipitate $(1\,1\,0)_{Mg_{17}Al_{12}}$ are in the plane of the page. From symmetry arguments, the Burgers OR has six variants given by the threefold substitution of $[\bar{1}\,\bar{1}\,2\,0]_{Mg}$, $[2\,\bar{1}\,\bar{1}\,0]_{Mg}$ and $[\bar{1}\,2\,\bar{1}\,0]_{Mg}$, combined with the twofold substitution of

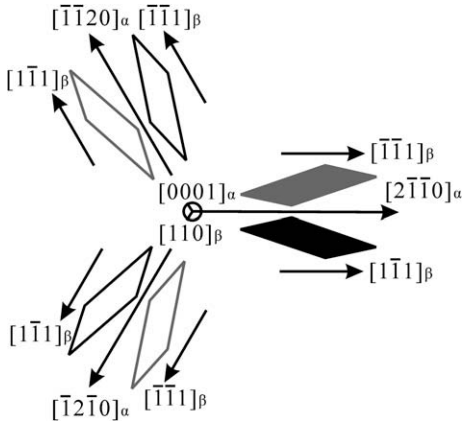

Fig. 12. A schematic representation of six variants of Burgers OR between $Mg_{17}Al_{12}$ phase (β) and Mg matrix (α) [63].

$[\bar{1}\,\bar{1}\,1]_{Mg_{17}Al_{12}}$ and $[1\,\bar{1}\,1]_{Mg_{17}Al_{12}}$ [63,64]. Fig. 9c shows that the microstructures consisting of long laths parallel to the basal plane formed a Widmanstätten morphology. A similar result has been observed by Celotto [63].

In this work, the CP exhibited a Burgers OR: $(0\,0\,0\,1)_{Mg}\|(1\,1\,0)_{Mg_{17}Al_{12}}$ and $[\bar{1}\,2\,\bar{1}\,0]_{Mg}\|[1\,\bar{1}\,1]_{Mg_{17}Al_{12}}$ (Fig. 10b). Unlike precipitation reactions in Al alloys where the equilibrium phase is usually preceded by at least one metastable allotrope, the $Mg_{17}Al_{12}$ phase forms directly from the supersaturated parent phase with an approximately homogeneous distribution [64]. HREM observations indicated that the $Mg_{17}Al_{12}$ lattice was undistorted, whereas in the Mg matrix a thin region in the vicinity of the interface appeared to be distorted (Fig. 10b). A similar phenomenon has been also observed in a Mg–10Al (at.%) alloy by Duly et al. [65].

5. Conclusions

1. Both the Pre-ST FSP and two-pass FSP resulted in the generation of uniform recrystallized microstructures in an AZ80 casting with grain sizes of 7.5–8.7 μm, characterized by dominant HAGBs of 95.9–97.5%; however, the boundary misorientation distributions were quite different for the two samples.
2. The microstructure of the Pre-ST FSP sample was characterized by a significant proportion of $\{10\bar{1}2\}$ twins and weakened texture component. The mechanism of DRX was mainly associated with TDRX and CDRX.
3. In the two-pass FSP sample, the microstructure was characterized by serrated recrystallized grains and weakened simple $\langle 0\,0\,0\,2\rangle$ texture component. The mechanism of DRX was mainly associated with CDRX and DDRX.
4. The difference in DRX between the Pre-ST FSP and two-pass FSP samples was mainly attributed to significant differences in initial grain sizes prior to final FSP. Large grains were beneficial to deformation twinning.
5. A post-FSP aging resulted in the precipitation of fine $Mg_{17}Al_{12}$ particles in continuous and discontinuous forms, and peak hardness was attained at 177 °C for 10 h.
6. The CP exhibited a Burgers OR, namely: $(0\,0\,0\,1)_{Mg}\|(1\,1\,0)_{Mg_{17}Al_{12}}$ and $[\bar{1}\,2\,\bar{1}\,0]_{Mg}\|[1\,\bar{1}\,1]_{Mg_{17}Al_{12}}$

Acknowledgments

The authors gratefully acknowledge the support of (a) the National Outstanding Young Scientist Foundation of China under Grant No. 50525103, (b) the National Basic Research Program of China under Grant No. 2006CB605205, (c) the National High-tech Research Program under Grant No. 2006AA03Z111, (d) the Hundred Talents Program of Chinese Academy of Sciences, and (e) China Postdoctoral Science Foundation for A.H.F.

References

[1] Honeycombe RWK. The plastic deformation of metals. London: Edward Arnold; 1971.
[2] Samman TA, Gottstein G. Mater Sci Eng 2008;A488:406.
[3] Galiyev A, Kaibyshev R, Gottstein G. Acta Mater 2001;49:1199.
[4] Sitdikov O, Kaibyshev R. Mater Trans 2001;42:1928.
[5] Li B, Ma E, Ramesh KT. Metall Mater Trans 2008;39A:2607.
[6] Christian JW, Mahajan S. Prog Mater Sci 1995;39:1.
[7] Yoo MH. Metall Trans 1981;12A:409.
[8] Humphreys FJ, Hatherly M. Recrystallization and related annealing phenomena. 2nd ed. Amsterdam: Elsevier; 2004.
[9] ASM Speciality Handbook. Magnesium and magnesium alloys. Materials Park (OH): ASM International; 1999.
[10] Sastry DH, Prasad YVRK, Vasu KI. Scripta Metall 1969;3:927.
[11] Sitdikov O, Kaibyshev R, Sakai T. Mater Sci Forum 2003;419–422:521.
[12] Meyers MA, Vohringer O, Lubarda VA. Acta Mater 2001;49:4025.
[13] Jiang L, Jonas JJ, Luo AA, Sachdev AK, Godet S. Mater Sci Eng 2007;A445–446:302.
[14] Thomas WM, Nicholas ED, Needham JC, Murch MG, Templesmith P, Dawes CJ.; G B Patent Application No. 9125978.8, December 1991.
[15] Mishra RS, Ma ZY. Mater Sci Eng 2005;R50:1.
[16] Ma ZY. Metall Mater Trans 2008;39A:642.
[17] Ma ZY, Mishra RS. Scripta Mater 2005;53:75.
[18] Mishra RS, Ma ZY, Charit I. Mater Sci Eng 2003;A341:307.
[19] Ma ZY, Pilchak AL, Juhas MC, Williams JC. Scripta Mater 2008;58:361.
[20] Lee CJ, Huang JC, Du XH. Scripta Mater 2007;56:875.
[21] Darras BM, Khraisheh MK, Farha FKA, Omar MA. J Mater Process Technol 2007;191:77.
[22] Chang CI, Du XH, Huang JC. Scripta Mater 2007;57:209.
[23] Woo W, Choo H, Brown DW, Liaw PK, Feng Z. Scripta Mater 2006;54:1859.
[24] Cavaliere P, Marco PPD. J Mater Process Technol 2007;184:77.
[25] Feng AH, Ma ZY. Scripta Mater 2007;56:397.
[26] Feng AH, Ma ZY. Metall Mater Trans A, in press.
[27] Valle JAD, Prado MTP, Ruano OA. Rev Metal Madrid 2002;38:353.
[28] Carter CB, Norton MG. Ceramic materials science and engineering. Berlin: Springer Verlag; 2007. pp. 246–268.
[29] Hill RER, Abbaschian R. Physical metallurgy principles. 3rd ed. Boston, MA: PWS-Kent Publishing Company; 1992.
[30] Cho JH, Dawson PR. Metall Mater Trans 2006;37A:1147.

[31] Kang SH, Bang WH, Cho JH, Han HN, Oh KH, Lee CG, Kim SJ. Mater Sci Forum 2005;495–497:901.
[32] Stanford N. Philos Mag Lett 2008;88:379.
[33] Nave MD, Barnett MR. Scripta Mater 2004;51:881.
[34] Taylor GI. J Inst Met 1938;62:307.
[35] Wonsiewicz BC, Backofen WA. Trans Metall Soc AIME 1967;239:1422.
[36] Valle JAD, Prado MTP, Ruano OA. Metall Mater Trans 2005;36A:1427.
[37] Su CW, Lu L, Lai MO. Philos Mag 2008;88:181.
[38] Kaibyshev RO, Sitdikov OS. Phys Met Metallogr 2000;89:384.
[39] Ion SE, Humphreys FJ, White SH. Acta Metall 1982;30:1909.
[40] Kaibyshev RO, Sitdikov OS. Phys Met Metallogr 1992;73:635.
[41] Byrne JG. Recovery, recrystallization, and grain growth. New York: Macmillan; 1965. p. 60.
[42] Beck PA, Sperry PR. J Appl Phys 1950;21:150.
[43] Kaibyshev R, Sitdikov O. Z Metallk 1994;85:738.
[44] Galiyev A, Kaibyshev R, Sakai T. Mater Sci Forum 2003;419–422:509.
[45] Armstron RW, Worthington PJ. In: Rohde RW, Butcher BM, Holland JR, Karnes CH, editors. Metallurgical effects at high strain rates. New York: Plenum Press; 1973.
[46] Danaf EE, Kalidindi SR, Doherty RD. Metall Mater Trans 1999;30A:1223.
[47] Gray III GT. J Phys IV 1997;7:C3–423.
[48] Barnett MR, Keshavarz Z, Beer AG, Atwell D. Acta Mater 2004;52:5093.
[49] Wang YN, Huang JC. Acta Mater 2007;55:897.
[50] Yoo MH, Lee JK. Philos Mag 1991;63A:987.
[51] Tan JC, Tan MJ. Mater Sci Eng 2003;A339:124.
[52] Valiev RZ, Kaibyshev OA, Khannanov SK. Phys Status Solidi 1979;52A:447.
[53] Mabuchi M, Higashi K. Acta Mater 1996;44:4611.
[54] Duly D, Simon JP, Brechet Y. Acta Metall Mater 1995;43:101.
[55] Clark JB. Acta Metall 1968;16:141.
[56] Klinger LM, Brechet JM, Purdy GR. Acta Mater 1997;45:5005.
[57] Crawley AF, Lagowski B. Metall Trans 1974;5:949.
[58] Duly D, Brechet Y. Acta Metall Mater 1994;42:3035.
[59] Duly D, Cheynet MC, Brechet Y. Acta Metall Mater 1994;42:3843.
[60] Duly D, Cheynet MC, Brechet Y. Acta Metall Mater 1994;42:3855.
[61] Baumann SF, Michael J, Williams DB. Acta Metall 1981;29:1343.
[62] Crawley AF, Milliken KS. Acta Metall 1974;22:557.
[63] Celotto S. Acta Metall 2000;48:1775.
[64] Hutchinson CR, Nie JF, Gorsse S. Metall Mater Trans 2005;36A:2093.
[65] Duly D, Zhang WZ, Audier M. Philos Mag 1995;71:187.
[66] Zhang M, Zhang WZ, Ye F. Metall Mater Trans 2005;36A:1681.